Fuel 271 (2020) 117518

Contents lists available at ScienceDirect

Fuel

journal homepage: www.elsevier.com/locate/fuel

Full Length Article

Excess enthalpy combustion of methane-air in a novel micro non-premixed combustor with a flame holder and preheating channels

Jianlong Wan[a,*], Yongjia Wu[b], Haibo Zhao[a,*]

[a] State Key Laboratory of Coal Combustion, School of Energy and Power Engineering, Huazhong University of Science and Technology, Wuhan 430074, China
[b] School of Civil Engineering and Architecture, Wuhan University of Technology, Wuhan 430070, China

ARTICLE INFO

Keywords:
Micro combustion
Non-premixed flame
Flame holder
Preheating channel
Excess enthalpy combustion

ABSTRACT

A novel micro non-premixed combustor with a flame holder and preheating channels is developed to improve the non-premixed flame stabilization for the first time. The numerical results indeed show that the methane-air non-premixed flames can maintain stable with no flashback or pulsating flame even at the stoichiometric ratio compared to the premixed flame, which indicates that the flame stabilization in the present combustor is indeed excellent. The maximum flame temperature at each operating condition is higher than the corresponding adiabatic flame temperature. The excess enthalpy ratio (R_{eer}) is larger at a smaller nominal equivalence ratio (ϕ) and a bigger Reynolds number (Re), and the maximum R_{eer} reaches 36.7%. With the decrease of ϕ, the area of excess enthalpy zone increases at smaller Re (< 160), but expands firstly and then shrinks at a larger Re (≥ 160). In addition, some new non-premixed flame propagation characteristics are found. At the larger ϕ (> 0.6), the flame top presents the "Λ" shape, which is significantly different from the flame topology structure of methane/air premixed flame. The standoff distance (S_{root}) between the flame root and the flame holder at the larger Re decreases firstly and then increases with the decrease of ϕ, and the anomalous and non-monotonic S_{root} are both found. These interesting flame propagation features are reported for the first time for the micro non-premixed flame. Researchers can gain insight into micro non-premixed flame propagation characteristics under the competitive effect between the combustion reaction and mixed performance through the present work.

1. Introduction

Micro- and meso-scale combustion has received extensive attention in the past decades, mainly due to the much higher energy densities of hydrocarbon fuels as compared with the traditional batteries. Owing to this major advantage, combustion-based micro-power-generation devices are considered to be a viable alternative to provide power for micro-electro-mechanical systems [1]. However, the large heat loss to the environment and the short residence time of the fuel mixture make the flame easily lose stability and exhibit many unstable behaviors in micro combustors [1–3].

Flame holder (such as bluff-body [4,5] and cavity [6]) is an effective strategy to anchor the flame owing to the flow recirculation zone. Wan *et al.* [4] found that blow-off limits of hydrogen/air premixed flame can be remarkably extended in the micro combustor with the bluff body. The methane/air premixed flame can remain symmetrically stable within a wide operating range in a mesoscale combustor with cavities [6]. Ansari *et al.* [7] found that the flame can be well anchored by the cylindrical bluff-body in a micro plate combustor. The bluff-body ball also had a significant effect on improving the flame stabilization of methane/air premixed mixture [8]. Yang *et al.* [9,10] and Peng *et al.* [11] pointed out that the recirculation zone behind the backward-facing step can effectively improve the hydrogen/air premixed flame stabilization in the micro tube combustor. However, the flame holder cannot significantly extend the flammability limit of fuel mixture. Heat recirculation is a frequently adopted method to broaden the flammable range based on equivalence ratio. Kuo and Ronney [12] found that the flammable range of lean propane/air can be remarkably extended in a miniature combustor with the "Swiss-roll" configuration. Veeraragavan [13,14] developed a micro plate burner made of the solid material of orthotropic thermal conductivity, and the result indicated that the "hot pocket" in the wall is beneficial for improving the flame stabilization. Jiang *et al.* [15] pointed out that the methane/air premixed flame stability can be improved in a small combustor with porous wall via preheating the fresh fuel mixture and reducing the heat loss to the ambient environment. The above literature demonstrated that the heat recirculation effect could significantly extend the flammable limit of fuel mixture, but the flames cannot be well anchored in these

* Corresponding authors at: State Key Laboratory of Coal Combustion, Huazhong University of Science and Technology, 1037 Luoyu Road, Wuhan 430074. China.
E-mail addresses: jlw@hust.edu.cn (J. Wan), hzhao@mail.hust.edu.cn (H. Zhao).

https://doi.org/10.1016/j.fuel.2020.117518
Received 7 January 2020; Received in revised form 1 March 2020; Accepted 2 March 2020
Available online 16 March 2020
0016-2361/

combustors, which narrows the flame blow-off limit.

Therefore, it is spontaneously expected that the effective combination of flow recirculation effect and heat recirculation effect can both extend the flammability limit and flame blow-off limit. To achieve this, Wan *et al.* [16,17] previously developed a micro combustor with a plate flame holder and preheating channels, which indeed take full advantage of the heat recirculation and flow recirculation effects. The numerical results showed that the CH_4/air premixed flame stabilization could be significantly improved in this combustor [16,17]. However, when the equivalence ratio of fuel mixture was too large (near the stoichiometric ratio), the premixed flame easily flashed back, which was dangerous. For example, the flame with repetitive flashback and pulsating occurred within the equivalence ratio range of 0.75–1.3 at the Reynolds number of 80 in this combustor [18].

Therefore, the non-premixed combustor might be more suitable in practical application. Based on this idea, a novel micro non-premixed combustor with a flame holder and preheating channels was developed in this paper. More importantly, the present combustor can act as a model to study the propagation characteristics of non-premixed flame under the synergistic effect of the heat recirculation and flow recirculation. The present work reports the methane-air non-premixed combustion characteristics in this combustor. Some new and interesting flame propagation features are discovered for the first time which is not found in the premixed flame.

2. Numerical methods

2.1. Combustor geometry

The geometrical structure schematic of a symmetric combustor with a flame holder and preheating channels is displayed in Fig. 1. The solid walls of the combustor are divides into five segments: the flame holder, two exterior walls of the preheating channels, and the two combustion chamber walls (CCW). The gas flow channel is divided into six segments by six yellow lines: two preheating channels of air, one fuel channel, two mixed channels of fuel and air, and one combustion chamber. The wall thickness is 0.5 mm, and the inlet widths of the air and fuel are both 1.0 mm. The widths of preheating channels and the combustion chamber are 1.0 and 4.0 mm, respectively. Other geometrical dimensions are presented in Fig. 1.

2.2. Mathematical model

As the *Re* in the present combustor is small, the non-premixed flame maintains the laminar mode. Therefore, a two-dimensional state laminar model is employed in present work. The governing equations are displayed as follows:

$$\text{Continuity equation:}\frac{\partial}{\partial x}(\rho u)+\frac{\partial}{\partial y}(\rho v)=0 \tag{1}$$

$$\text{Momentum equations:}\frac{\partial(\rho uu)}{\partial x}+\frac{\partial(\rho uv)}{\partial y}=-\frac{\partial p}{\partial x}+\frac{\partial \tau_{xx}}{\partial x}+\frac{\partial \tau_{xy}}{\partial y} \tag{2}$$

$$\frac{\partial(\rho vu)}{\partial x}+\frac{\partial(\rho vv)}{\partial y}=-\frac{\partial p}{\partial y}+\frac{\partial \tau_{yx}}{\partial x}+\frac{\partial \tau_{yy}}{\partial y} \tag{3}$$

$$\text{Energy equation:}\frac{\partial(\rho uh)}{\partial x}+\frac{\partial(\rho vh)}{\partial y}=\frac{\partial(\lambda_f\partial T_f)}{\partial x^2}+\frac{\partial(\lambda_f\partial T_f)}{\partial y^2}+\sum_i\left[\frac{\partial}{\partial x}\left(h_i\rho D_{m,i}\frac{\partial Y_i}{\partial x}\right)+\frac{\partial}{\partial y}\left(h_i\rho D_{m,i}\frac{\partial Y_i}{\partial y}\right)\right]+\sum_i h_iR_i \tag{4}$$

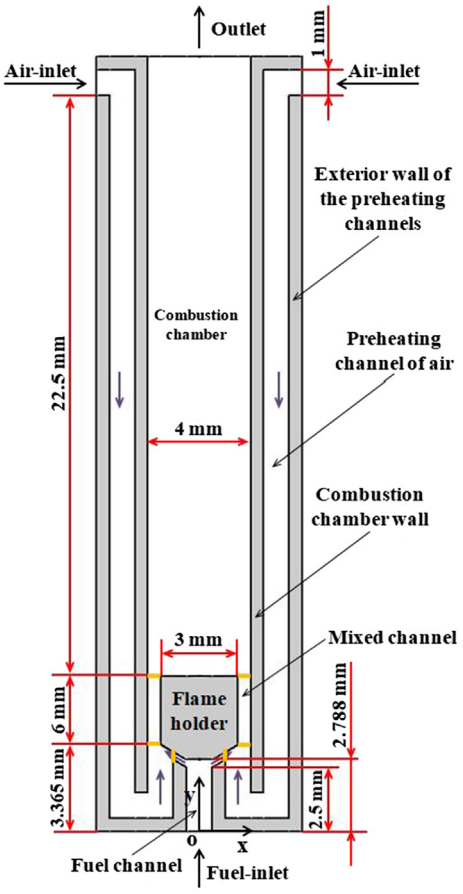

Fig 1. Geometrical structure of the micro non-premixed combustor with a flame holder and preheating channels.

$$\text{Species equation:}\frac{\partial(\rho Y_i u)}{\partial x}+\frac{\partial(\rho Y_i v)}{\partial y}=\frac{\partial}{\partial x}\left(\rho D_{m,i}\frac{\partial Y_i}{\partial x}\right)+\frac{\partial}{\partial y}\left(\rho D_{m,i}\frac{\partial Y_i}{\partial y}\right)+R_i \tag{5}$$

$$\text{Energy equation for the solidwalls:}\frac{\partial(\lambda_s\partial T_s)}{\partial x^2}+\frac{\partial(\lambda_s\partial T_s)}{\partial y^2}=0 \tag{6}$$

where u and v are the $\times$ and y components of the flow velocity, respectively; ρ and ρ_s are the densities of the fluid and solid wall, respectively; P is the fluid pressure; $D_{m,i}$ is the mass diffusion coefficient of species i; Y_i, h_i, and R_i are the mass fraction, formation enthalpy, and generation/consumption rate of species i, respectively; T_f and T_s are the fluid and solid wall temperatures, respectively; λ_f and λ_s are the thermal conductivities of the fluid and solid wall, respectively.

2.3. Computational scheme

The present combustor is made by the quartz glass, whose thermal conductivity is 2.0 W/(m·K) [19]. The methane at the fuel-inlet and air at the air-inlet were both set as the uniform velocity distributions of 300 K. The nominal equivalence ratio (ϕ) is the corresponding desired value when the methane and air are homogeneous mixed. Three Reynolds numbers (Re = 80, 160, and 240), which are calculated based on the characteristic length of 1.0 mm (the width of combustor inlet), are adopted as typical examples to reveal the combustion characteristics of methane-air in the present combustor. Maintaining a constant Re, the ϕ is decreased with a decrement of 0.025 from 1.0 until the flame blows off. The heat fluxes in both the solid walls and the fluid were computed using Fourier's law. The inner wall surface of the combustor was set as chemically inert and no-slip. A Neumann boundary was applied at the

outlet of the combustor. The heat loss from the outer wall to the ambient environment was calculated to be $q = h_s(T_{W,O} - T_\infty) + \varepsilon_s\sigma_s(T_{W,O}^4 - T_\infty^4)$, where $T_\infty = 300$ K (the ambient temperature), $T_{w,o}$ is the outer wall temperature, h_s is the heat transfer coefficient of natural convection (5.0 $W{\cdot}m^{-2}{\cdot}K^{-1}$) [20], ε_s is the wall surface emissivity (0.92) [21], and σ_s is the Stephan-Boltzmann constant (5.67 $\times$ 10^{-8} $W{\cdot}m^{-2}{\cdot}K^{-4}$).

ANSYS Fluent 14.0 is applied to solve the momentum, mass, energy, and species conservation equations [22]. The same numerical model was also adopted to simulate the methane/air premixed flame in a similar combustor presented in our previous work, and its accuracy had been confirmed by comparing the experimental and simulated flammability limits and exhaust gas temperatures at different *Re* and equivalence ratios [23]. A detailed DRM-19 chemistry mechanism (21 species and 84 reactions) is adopted to simulate the methane-air combustion reaction [24], and the thermodynamic and transport properties of the reaction species were taken from the CHEMKIN databases [25]. The fluid temperature in the combustion chamber is set as 2000 K to initiate the combustion reaction of the methane/air. Grid independence was checked using three sets of grid systems ($\Delta x = \Delta y$ = 25, 20, and 10 μm, respectively) (see Fig. 2). It is found that a cell size of 25 μm (~15 grids in the flame front) is sufficient to capture the flame structure by comparing the two key radical profiles (HCO and CO) near the flame front at $\phi = 1.0$ (the flame front is the thinnest at this case). A non-uniform grid system is finally employed. The convergence of the CFD simulation is judged based on the residuals to be less than 1.0 $\times$ 10^{-6}.

3. Results and discussion

3.1. Flame regime diagram

Fig. 3 shows a regime diagram of flame behavior at different *Re* and equivalence ratios. It should be pointed out that the flame can keep stable in the combustion chamber at the whole operating range of ϕ and *Re*, which is quite different from the premixed flame behaviors of methane/air in the micro combustors with a flame holder and preheating channels [18]. The numerical results in Ref. [18] demonstrated that there existed flashback phenomena and pulsating flames at some

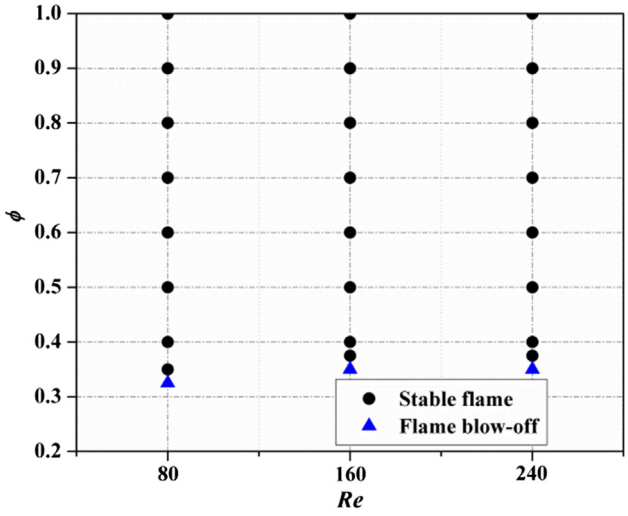

Fig 3. Regime diagrams of flame behavior for different *Re* and ϕ.

operating conditions in the micro premixed combustor, and the flashback phenomenon was also recently observed in the mesoscale combustor with a flame holder and preheating channels via experiment [23]. However, there are no flashback phenomenon and pulsating flame in present combustor even in the case of a stoichiometric ratio. Moreover, the flammability limit at each *Re* is also very small. These indicate that the flame stabilizations in the present non-premixed combustor are excellent. The following sections will show and discuss the combustion characteristics in this combustor.

3.2. Mixed performance of fuel and air

For the convenience of quantitative discussion, the flame front is defined at first. It has been confirmed that the mass fraction of HCO (Y_{HCO}) is appropriate to mark the flame front in the combustion processes of hydrocarbon fuels [26]. Here, the same definition is used. It is found that the high reaction rate zone of methane lies in the normalized

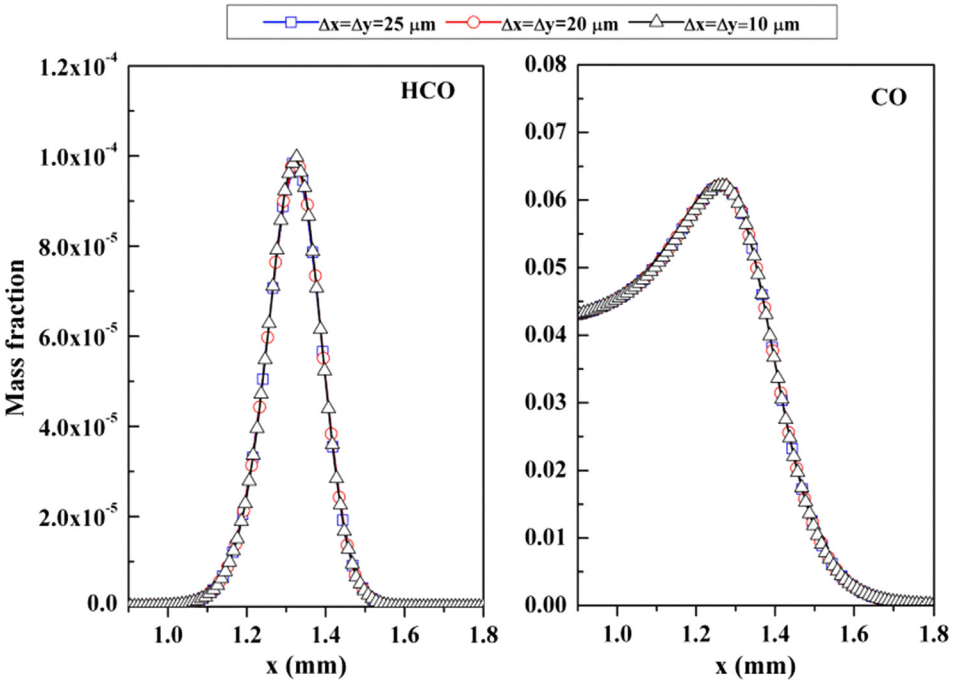

Fig 2. Mass fractions profiles of HCO and CO near the flame front (y = 7.0 mm) for three different grid resolutions at $\phi = 1.0$ and $Re = 160$.

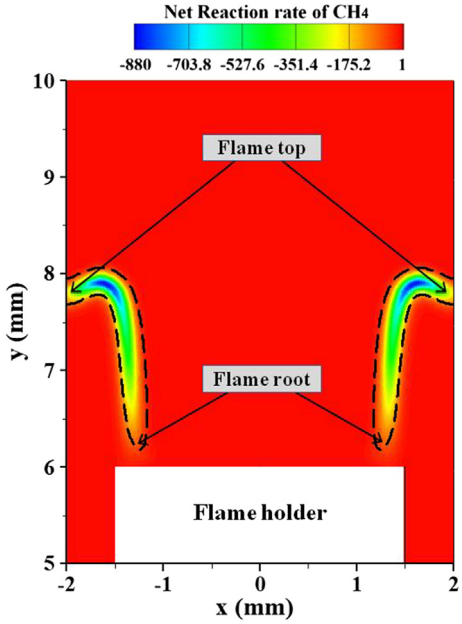

Fig 4. Net reaction rate contours of CH_4 with overlaid 10% maximum Y_{HCO} isoline (blue dashed line) at $\phi = 1.0$ and $Re = 160$. (For interpretation of the references to colour in this figure legend, the reader is referred to the web version of this article.)

isolines of 10% of maximum Y_{HCO} for all cases (see Fig. 4). Given this, the 10% isoline of maximum Y_{HCO} is used to visualize the flame front in the present work.

For non-premixed combustor, the mixed performance of fuel and air directly influences the combustion characteristics. Therefore, the mixed performance of fuel and air should be checked. In this combustor, the methane and air are drastically mixed around the outlet of fuel channel for all operating conditions mainly via convection, as shown in Fig. 5.

Subsequently, they are continuously mixing in the mixed channel mainly via diffusion. The case of $\phi = 1.0$ and $Re = 160$ is adopted as an example to quantitatively reveal the mixed performance of methane and air, as shown in Fig. 6. It can be seen that the difference between the local Y_{CH4} and the desired value at the homogeneous mixing is significantly decreasing with the downstream movement of fuel and air mixture. Moreover, the Y_{CH4} at the upstream and middle locations of the mixed channel ($y = 4.0$ and 5.0 mm) is decreasing along with the y section towards CCW. However, the Y_{CH4} at the outlet of mixed channel ($y = 6.0$ mm) increases firstly and then decreases. It is known that the diffusion velocity of methane is positive correlation with its concentration and temperature. Here, the methane temperature very near the vertical wall of flame holder ($x = 1.5$ mm) is obviously higher than that near the middle location ($y = 1.75$ mm) due to the preheating effect of flame holder, and the difference between them is larger in the more downstream channel (their differences at $y = 4.0$, 5.0, and 6.0 mm are 69.0, 122.8, and 180.7 K, respectively). Fig. 6 also quantitatively shows the laminar diffusion coefficient of CH_4 at different y sections. It can be seen that the diffusion velocity of methane very near the flame holder is indeed faster than that near the middle location. In the mixed channel, the methane with a faster diffusion velocity very near the flame holder diffuses towards the x positive direction. In the meantime, the methane with a relatively slower diffusion velocity around the middle of mixed channel also diffuses towards the x positive direction. The difference of diffusion velocity between them will results in the temporary gather of methane near the middle of the left half of mixed channel ($y = 1.625$ mm) when the difference between the local Y_{CH4} and the desired value is small enough, which is also observed in other operating conditions.

When the methane-air mixture flows out of the mixed channel, they will further mix in the combustion chamber before combustion. Fig. 7 presents that there are closed Y_{CH4} isolines before the flame front, and the upstream boundary of the flame front is nearly parallel to the closed Y_{CH4} isolines around the flame front. This means that methane and air are almost homogeneous mixed before combustion. Compared with premixed flame, non-premixed flames are significantly influenced by the mixed performance of fuel and air at some operating conditions, which will be reflected in the thermal performance and flame behavior.

3.3. Excess enthalpy combustion performance

The excess enthalpy ratio and excess enthalpy zone was defined for the convenience of quantitative discussion. The excess enthalpy ratio $R_{eer} = (T_f\text{-}T_{ad})/T_{ad}$: T_f is the actual maximum flame temperature; T_{ad} is the corresponding adiabatic flame temperature. The excess enthalpy zone is defined as the zone where the gaseous mixture temperature is higher than the T_{ad}. It can be seen from Fig. 8 that the temperature level of the combustor significantly decreases with the decreasing ϕ under a constant Re or the increasing Re under a constant ϕ. Besides, the area of excess enthalpy zone is also significantly influenced by the Re and ϕ, which will be quantitatively calculated in the following section.

To analyze the preheating performance on the fuel mixture, Fig. 9 shows the gas temperature profiles at the inlet of combustion chamber. As it is observed, the unburned fuel mixture temperature decreases more quickly with decreased ϕ. The mixture temperature near the flame holder ($x = 1.5$ mm) is larger than that near the CCW ($x = 2.0$ mm), especially for the smaller ϕ, which means that the preheating effect of flame holder on fresh fuel mixture is more significant compared with the CCW at smaller ϕ. Under a constant ϕ, the unburned fuel mixture temperature increases with the decreasing Re mainly due to the lower flame height at smaller Re. It is known that a higher preheating temperature of fuel mixture is beneficial for improving the excess enthalpy

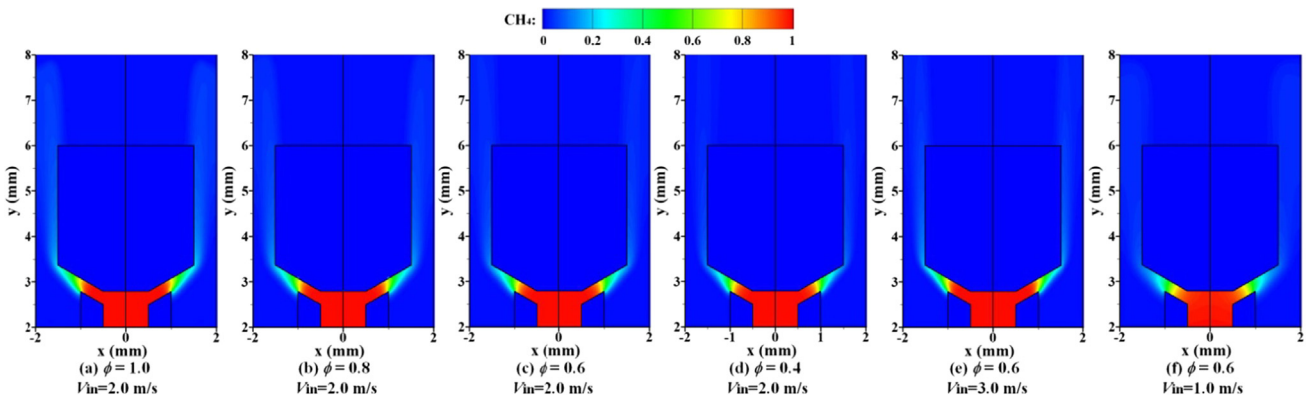

Fig 5. Mass fraction contours of CH_4 near the flame holder for different ϕ and Re.

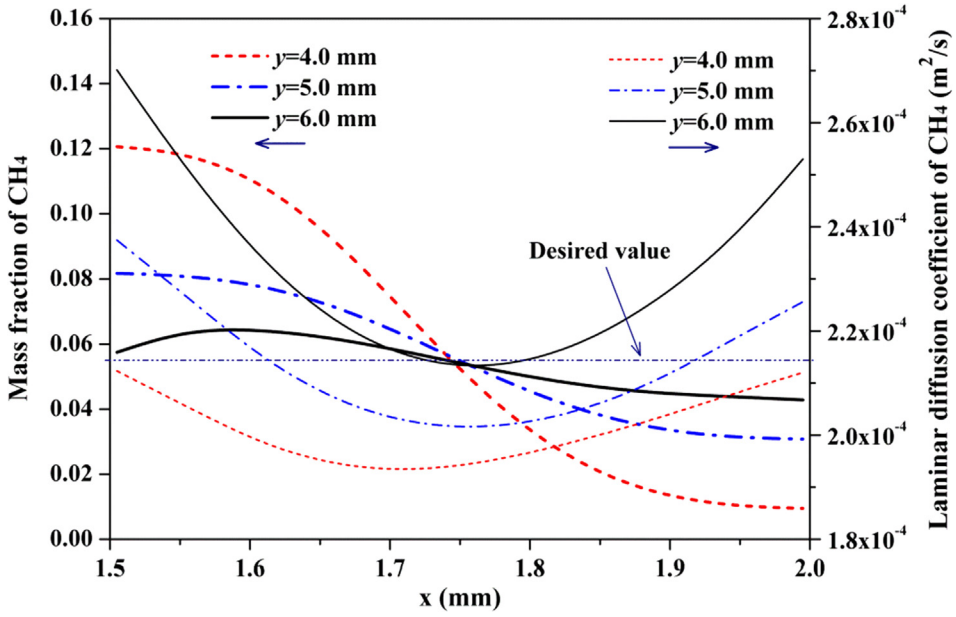

Fig 6. Y_{CH4} and the laminar diffusion coefficient of CH_4 profiles at different y sections in the mixed channel at $\phi = 1.0$ and $Re = 160$.

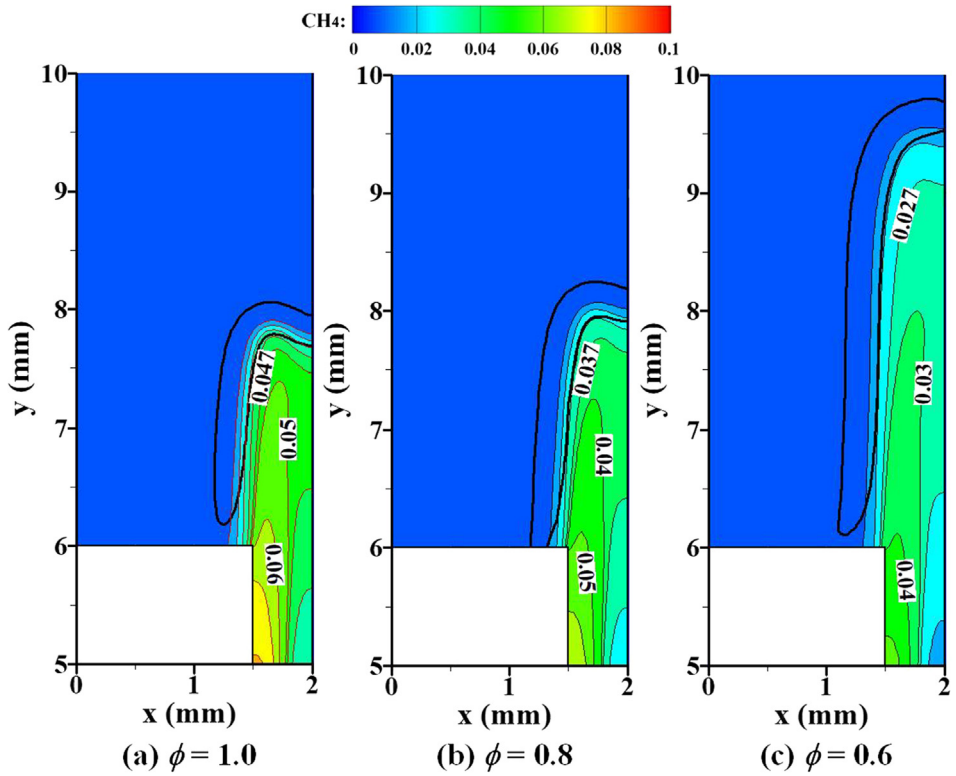

Fig 7. Y_{CH4} contours and isolines overlaid with the 10% maximum Y_{HCO} isolines (solid black lines) for different ϕ at $Re = 160$.

combustion, but the T_{max} and R_{eer} are smaller for a smaller Re (see Fig. 10). This means that the heat recirculation effect of preheating channel on the gaseous mixture is not the main factor in determining the excess enthalpy combustion characteristic.

Fig. 10 presents the maximum flame temperature, excess enthalpy ratio, and the area of excess enthalpy zone to quantitatively evaluate the non-premixed combustion performance in the combustion chamber. It can be seen that the decreasing amplitude of T_f increases with a decreasing ϕ, but the T_f at each ϕ and Re is larger than the corresponding T_{ad}. Moreover, the T_f at a larger Re is higher. Interestingly, for a larger ϕ (> 0.6), the differences of T_f at $Re = 160$ and 240 are small (for example, T_f at $Re = 160$ and 240 under $\phi = 1.0$ are 2420.0 and 2424.1 K, respectively); for a smaller ϕ (< 0.6), the differences of T_f at $Re = 80$ and 160 are small (for example, T_f at $Re = 80$ and 160 under $\phi = 0.4$ are 1583.0 and 1585.2 K, respectively). This is mainly because that the combustion efficiency at $\phi > 0.6$ is high (~100%, see Fig. S1 in Supplemental Material (SM)), and the flame height are all low (< 4.0 mm, see Fig. 12b). This means that the heat release zones (i.e., combustion reaction zones) are small, so the increase of Re (i.e., the increase of fuel amount) in a certain range (from $Re = 80$ to 160) can

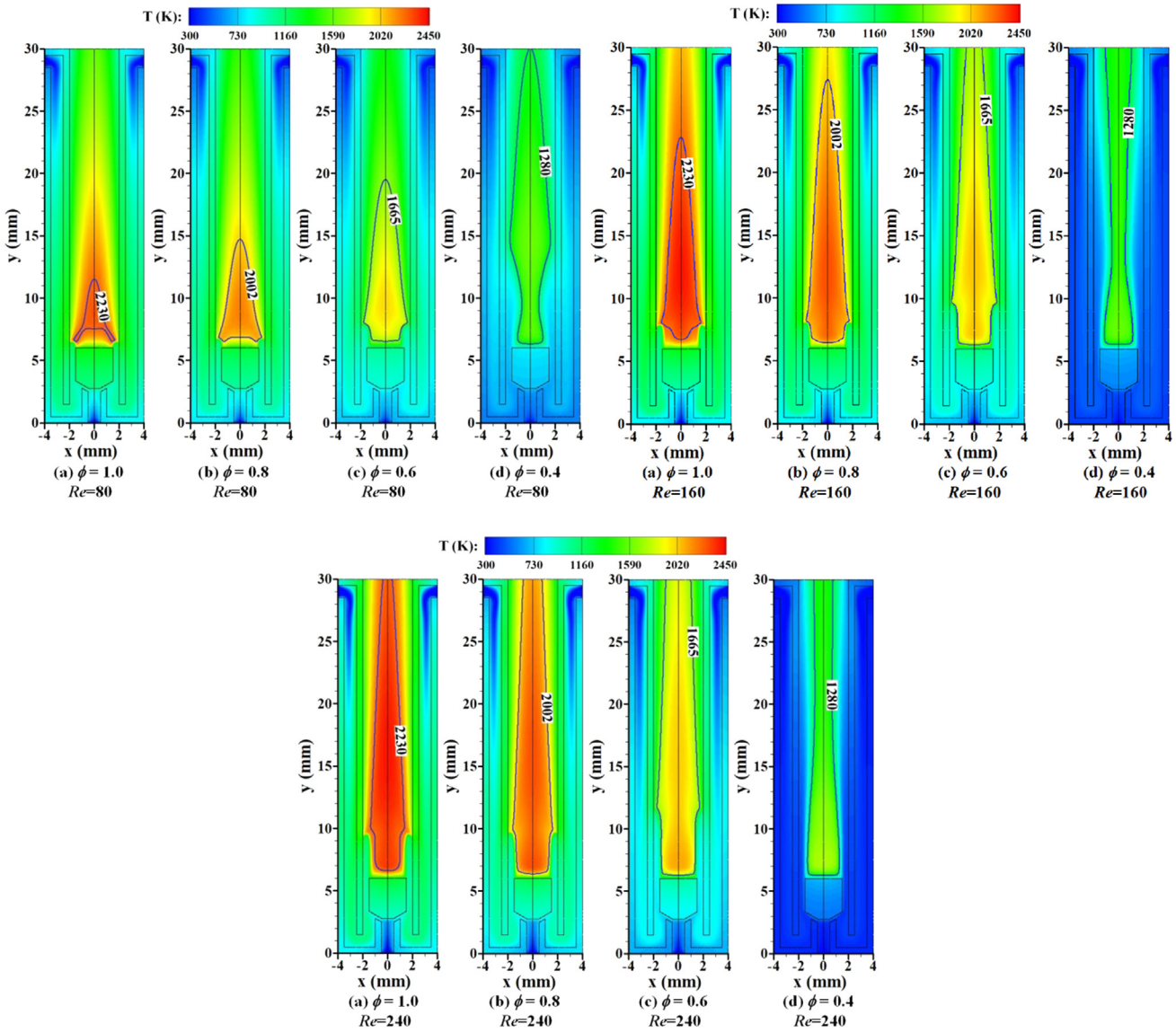

Fig 8. Temperature contours of the combustor overlaid with the corresponding adiabatic flame temperature [27] isoline for different ϕ and *Re*.

remarkably enhance the combustion intensity (see Fig. S2 in SM), which significantly increases the T_f. When the *Re* is large enough, the increase of *Re* is insignificant for enhancing the combustion intensity, so that the increase of T_f is very small. For a smaller equivalence ratio ($\phi < 0.6$), the flame behavior at $Re = 160$ and 240 are narrow and long. And the flame tops close to the outlet of combustor. But the flame roots still very close to the flame holder. The decrease in *Re* can significantly weaken the combustion intensity, which leads to the obvious decrease of T_f from $Re = 240$ to 160. When the *Re* continuously decreases to 80, the flame top remarkably shifts upstream, which results in a shorter flame (see Fig. 11f) and high combustion efficiency, so that the decrease of T_f from $Re = 160$ to 80 is very small. Besides, Fig. 10b shows the corresponding excess enthalpy ratio, which demonstrates that the R_{eer} increases with the decrease of ϕ, and the maximum R_{eer} can reach 36.7%. This means that the combustion reaction in present combustor is very intense, and the excess enthalpy combustion is more obvious at a smaller ϕ. Fig. 10c presents that, with the decrease of ϕ, the area of excess enthalpy zone at $Re = 80$ increases. But it increase firstly and then decrease at $Re = 160$ and 240. This is mainly because that the combustion efficiencies at $Re = 160$ and 240 under $\phi = 0.4$ decrease sharply.

3.4. Anchoring locations of the flame

Fig. 11 shows the flow field overlaid with 10% maximum Y_{HCO} isolines. It is seen that the flame top at larger ϕ (> 0.6) presents the "Λ" shape, which is significantly different from the flame topology structure of methane/air premixed flame in a similar combustor [16,23]. However, the flame behavior at smaller ϕ (≤0.6) is similar to the corresponding premixed flame behavior [23]. Fig. 11 also shows that the flame front is higher at a smaller ϕ or a larger *Re*. The quantitative information about the anchoring locations of flame root and top as well as the flame height is presented in Fig. 12 in detail.

In Fig. 12a, it is interesting to find that, with the decrease of ϕ under a constant *Re*, the standoff distance between the flame root and the upper wall of the flame holder (S_{root}) at $Re = 80$ increases. But it decreases firstly and then increase at $Re = 160$ and 240. This is a new feature for the micro methane-air non-premixed flame, which has not been reported so far. For the premixed flame in a similar combustor, the S_{root} is increasing with the decreasing ϕ all the time [23], because the anchoring location of flame root in present case is not only influenced by the combustion intensity, which is positive correlation with the ϕ, but also determined by the mixed performance of fuel and air at different ϕ. For the larger *Re* (> 80), the mixed time of fuel and air in the

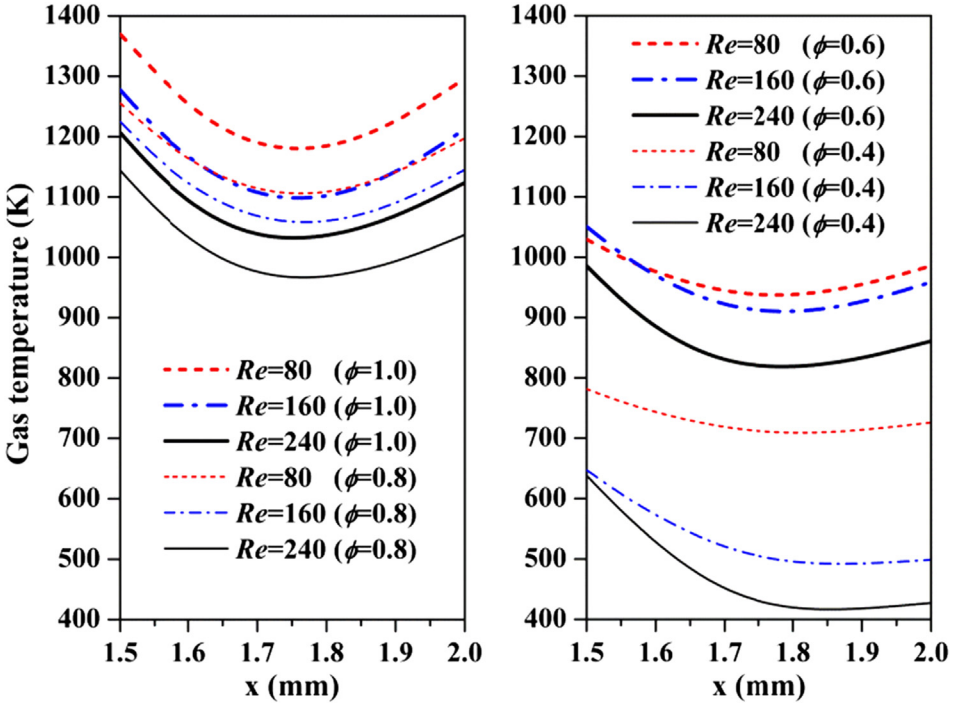

Fig 9. Gas temperature profiles at the inlet of the combustion chamber (y = 6.0 mm) for different ϕ and Re.

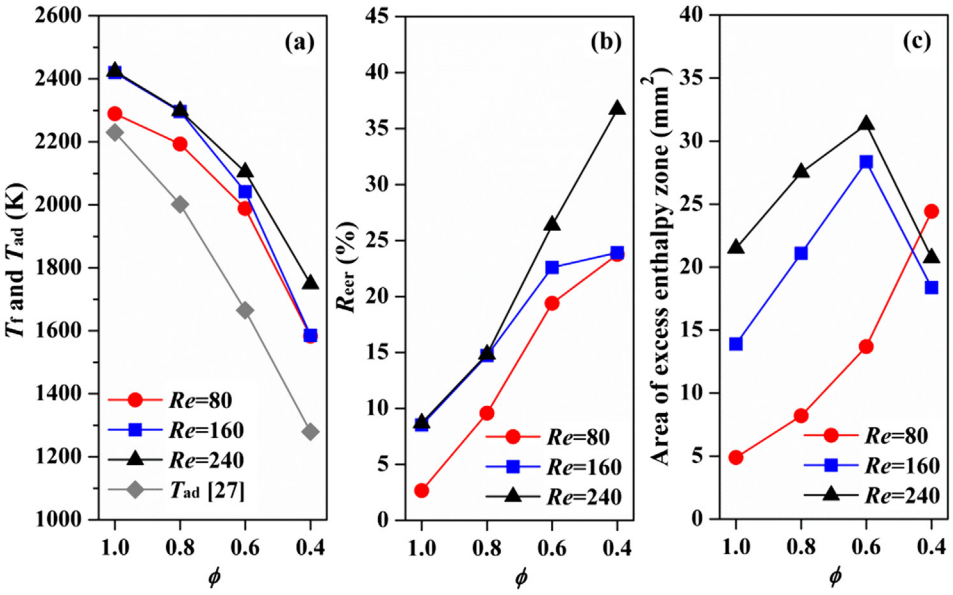

Fig 10. Maximum flame temperature (T_f) and the corresponding adiabatic flame temperature(T_{ad}) [27] (a), excess enthalpy ratio (b), and area of excess enthalpy zone (c) for different ϕ and Re.

mixed channel is shorter, and the fuel and air at the larger ϕ need more time to be homogeneously mixed in the combustion chamber before combustion. As a result, the flame roots at the larger ϕ under a bigger Re stay at a more downstream location, which results in the non-monotonic S_{root} at Re = 160 and 240. In addition, with the increase of Re under a constant ϕ, the S_{root} at ϕ > 0.6 increases (the normal S_{root}). But it decreases at ϕ = 0.6 (the anomalous S_{root} [28]). The anomalous S_{root} in Ref. [28] were observed in the mesoscale tube combustor with a central rod using the CH_4/H_2/air premixed flame at Lewis number Le < 1.0 due to the preferential transport effect, which is different from the underlying mechanisms of present anomalous S_{root}. At ϕ = 0.4, the S_{root} increases firstly and then decreases with the increase of Re, which was recently observed for the methane/air premixed flame in the similar combustor via experiment by us (see Fig. S3 in SM). To the best our knowledge, it is the first time to report the anomalous and non-monotonic S_{root} for a non-premixed flame of methane-air at $Le \approx$ 1.0. Fig. 12a also demonstrates that the flame top obviously shifts downstream with an increasing Re or a decreasing ϕ. As a result, the flame height is higher at a larger Re or a smaller ϕ (see Fig. 12b). It should be pointed out that the flame height sharply increases from ϕ = 0.6 to 0.4, which means that the combustion stabilization in the combustion chamber significantly reduces at ϕ = 0.4.

4. Conclusions

A novel micro non-premixed combustor which has a flame holder

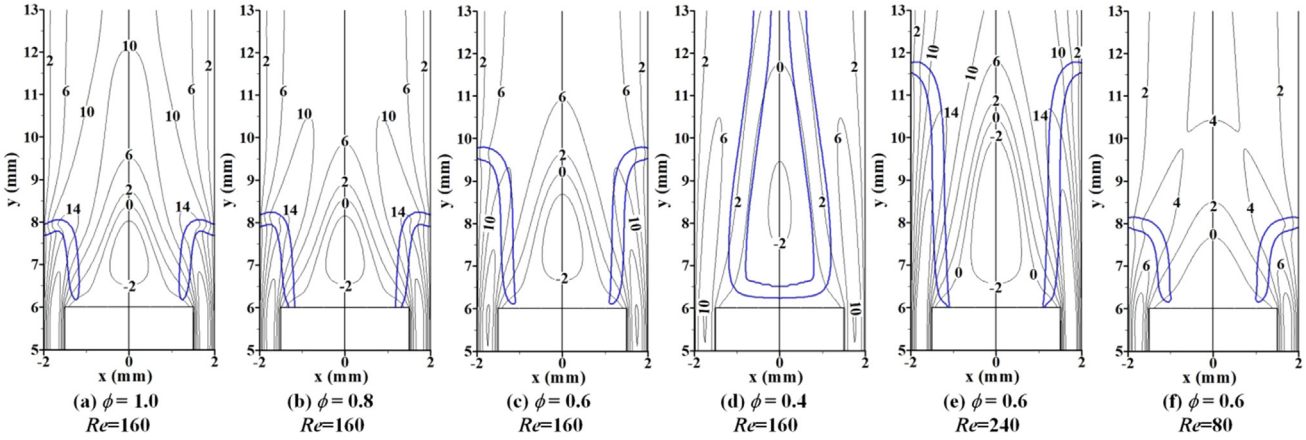

Fig 11. Flow field overlaid with 10% maximum Y_{HCO} isolines (blue solid lines) for different ϕ and *Re*. (For interpretation of the references to colour in this figure legend, the reader is referred to the web version of this article.)

and preheating channels is developed in the present work. The excess enthalpy combustion characteristics of methane-air are studied for this combustor. The result shows that the non-premixed flame maintains stable (no flashback phenomenon or pulsating flame even at the stoichiometric ratio) in the combustion chamber over a wide operating range, which indicates that the flame stabilizations in the present combustor is indeed excellent. The mixed performance of fuel and air, excess enthalpy combustion performance, and anchoring locations of the flame are revealed, and some new features of flame propagation are identified. For the mixed performance of fuel and mixture, the difference between the local Y_{CH4} and the desired value significantly decreases along with the downstream flow in the mixed channel, and they are further mixed in the combustion chamber until almost homogeneously mixed before the combustion. Moreover, the T_f at each ϕ and *Re* is larger than the corresponding T_{ad}. The R_{eer} increases with the decreasing ϕ or the increasing *Re*, and the maximum R_{eer} reaches 36.7%, which means that the combustion reaction in present combustor is very intense. With the decrease of ϕ, the area of excess enthalpy zone at $Re = 80$ increases. But it increases firstly and then decreases at $Re = 160$ and 240. Furthermore, the flame top at larger ϕ (> 0.6) presents the "Λ" shape, which is significantly different from the flame topology structure of methane/air premixed flame in a similar combustor. It is interesting to find that the S_{root} at $Re = 160$ and 240 decrease firstly and then increases with smaller ϕ, which has not been reported so far. The anomalous and non-monotonic S_{root} for the methane-air non-premixed flame are also reported for the first time. The present work helps the researchers to gain more insight into the micro non-premixed flame propagation characteristics.

CRediT authorship contribution statement

Jianlong Wan: Conceptualization, Methodology, Formal analysis, Investigation, Data curation, Writing - original draft, Visualization. **Yongjia Wu:** Writing - original draft, Writing - review & editing. **Haibo Zhao:** Writing - review & editing, Validation, Supervision.

Declaration of Competing Interest

The authors declare that they have no known competing financial interests or personal relationships that could have appeared to influence the work reported in this paper.

Acknowledgments

This work was supported by the National Natural Science Foundation of China (No. 51706080).

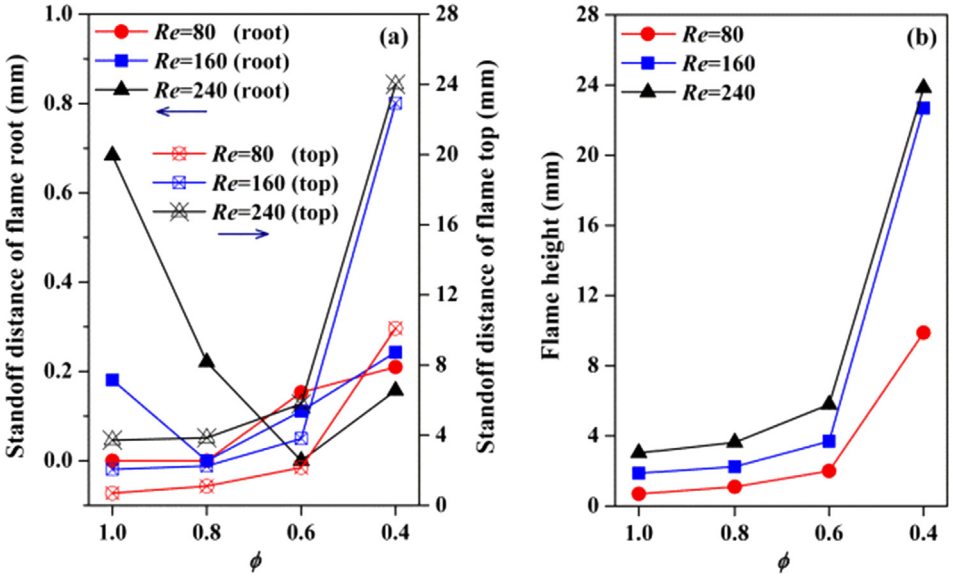

Fig 12. Standoff distance between the flame root/flame top and flame holder (a), and the flame height (b) for different ϕ and *Re*.

Appendix A. Supplementary data

Supplementary data to this article can be found online at https://doi.org/10.1016/j.fuel.2020.117518.

References:

[1] Ju Y, Maruta K. Microscale combustion: Technology development and fundamental research. Prog Energ Combust Sci 2011;37:669–715.
[2] Maruta K, Kataoka T, Kim NI, Minaev S, Fursenko R. Characteristics of combustion in a narrow channel with a temperature gradient. Proc Combust Inst 2005;30:2429–36.
[3] Wan JL, Shang C, Zhao H. Dynamics of methane/air premixed flame in a mesoscale diverging combustor with/without a cylindrical flame holder. Fuel 2018;232:659–65.
[4] Wan JL, Fan AW, Maruta K, Yao H, Liu W. Experimental and numerical investigation on combustion characteristics of premixed hydrogen/air flame in a micro-combustor with a bluff body. Int J Hydrogen Energ 2012;37:19190–7.
[5] Wan JL, Cheng X. Numerical investigation of the local extinction and re-ignition mechanisms of premixed flame in a micro combustor with a flame holder and preheating channels. Fuel 2020;264:116837.
[6] Wan JL, Fan AW, Liu Y, Yao H, Liu W, Gou XL, et al. Experimental investigation and numerical analysis on flame stabilization of CH4/air mixture in a mesoscale channel with wall cavities. Combust Flame 2015;162:1035–45.
[7] Ansari M, Amani E. Micro-combustor performance enhancement using a novel combined baffle-bluff configuration. Chem Eng Sci 2018;175:243–56.
[8] Pan J, Zhang C, Pan Z, Wu D, Zhu Y, Lu Q, et al. Investigation on the effect of bluff body ball on the combustion characteristics for methane/oxygen in micro combustor. Energ 2020;190:116465.
[9] Yang WM, Chou SK, Shu C, Xue H, Li ZW, Li DT, et al. Microscale combustion research for application to micro thermophotovoltaic systems. Energ Convers Manage 2003;44:2625–34.
[10] Yang WM, Chua KJ, Pan JF, Jiang DY, An H. Development of micro-thermophotovoltaic power generator with heat recuperation. Energ Convers Manage 2014;78:81–7.
[11] Peng Q, Chen JEJ, Zuo W, Zhao X, Zhang Z. Investigation on the effects of wall thickness and porous media on the thermal performance of a non-premixed hydrogen fueled cylindrical micro combustor. Energ Convers Manage 2018;155:276–86.
[12] Kuo CH, Ronney PD. Numerical modeling of non-adiabatic heat-recirculating combustors. Proc Combust Inst 2007;31:3277–84.
[13] Veeraragavan A. On flame propagation in narrow channels with enhanced wall thermal conduction. Energ 2015;93:631–40.
[14] Veeraragavan A, Cadou CP. Flame speed predictions in planar micro/mesoscale combustors with conjugate heat transfer. Combust Flame 2011;158:2178–87.
[15] Jiang LQ, Zhao DQ, Wang XH, Yang WB. Development of a self-thermal insulation miniature combustor. Energ Convers Manage 2009;50:1308–13.
[16] Wan JL, Fan AW. Effect of solid material on the blow-off limit of CH4/air flames in a micro combustor with a plate flame holder and preheating channels. Energ Convers Manage 2015;101:552–60.
[17] Wan JL, Fan AW, Yao H. Effect of the length of a plate flame holder on flame blowout limit in a micro-combustor with preheating channels. Combust Flame 2016;170:53–62.
[18] Wan JL, Zhao H. Dynamics of premixed CH 4 /air flames in a micro combustor with a plate flame holder and preheating channels. Energ 2017;139:366–79.
[19] Xu B, Ju Y. Experimental study of spinning combustion in a mesoscale divergent channel. Proc Combust Inst 2007;31:3285–92.
[20] Holman JP. Heat transfer. 9th ed. New York: McGraw-Hill; 2002.
[21] Ma Q, Fang R, Xiang L. Handbook of thermo-physical properties. Bejing: China Agricultural Machinery Press (in chinese); 1986.
[22] Fluent 14.0. User's Guide, Canonsburg, PA, 2011.
[23] Wan JL, Xu Z, Zhao H. Methane/air premixed flame topology structure in a mesoscale combustor with a plate flame holder and preheating channels. Energ 2018;165:802–11.
[24] Kazakov A, Frenklach M. Reduced Reaction Sets based on GRI-Mech 1.2, a 19-species reaction set. Accessed April; 2019.
[25] RJ Kee, JF Grcar, MD Smooke, JA Miller. Sandia National Laboratories Report, SAND85-8240; 1994.
[26] Kedia KS, Ghoniem AF. The anchoring mechanism of a bluff-body stabilized laminar premixed flame. Combust Flame 2014;161:2327–39.
[27] http://vbt.ebi.kit.edu/index.pl/html/equ/. Accessed May 2019.
[28] Shoshin Y, Bastiaans RJM, de Goey LPH. Anomalous blow-off behavior of laminar inverted flames of ultra-lean hydrogen–methane–air mixtures. Combust Flame 2013;160:565–76.